Derya Karabulut
Department of Mechanical Engineering,
Faculty of Engineering,
Istanbul University-Cerrahpasa,
Avcilar, Istanbul 34320, Turkey
e-mail: deryakarabulut@istanbul.edu.tr

Suzan Cansel Dogru
Department of Mechanical Engineering,
Faculty of Engineering,
Istanbul University-Cerrahpasa,
Avcilar, Istanbul 34320, Turkey
e-mail: cansel.gurcan@istanbul.edu.tr

Yi-Chung Lin
Department of Mechanical Engineering,
University of Melbourne,
Parkville, Victoria 3010, Australia
e-mail: linyc@unimelb.edu.au

Marcus G. Pandy
Department of Mechanical Engineering,
University of Melbourne,
Parkville, Victoria 3010, Australia
e-mail: pandym@unimelb.edu.au

Walter Herzog
Human Performance Laboratory,
The University of Calgary,
Calgary, AB T2N 1N4, Canada
e-mail: wherzog@ucalgary.ca

Yunus Ziya Arslan[1]
Department of Mechanical Engineering,
Faculty of Engineering,
Istanbul University-Cerrahpasa,
Avcilar, Istanbul 34320, Turkey
e-mail: yzarslan@istanbul.edu.tr

Direct Validation of Model-Predicted Muscle Forces in the Cat Hindlimb During Locomotion

Various methods are available for simulating the movement patterns of musculoskeletal systems and determining individual muscle forces, but the results obtained from these methods have not been rigorously validated against experiment. The aim of this study was to compare model predictions of muscle force derived for a cat hindlimb during locomotion against direct measurements of muscle force obtained in vivo. The cat hindlimb was represented as a 5-segment, 13-degrees-of-freedom (DOF), articulated linkage actuated by 25 Hill-type muscle-tendon units (MTUs). Individual muscle forces were determined by combining gait data with two widely used computational methods—static optimization and computed muscle control (CMC)—available in OPENSIM, an open-source musculoskeletal modeling and simulation environment. The forces developed by the soleus, medial gastrocnemius (MG), and tibialis anterior muscles during free locomotion were measured using buckle transducers attached to the tendons. Muscle electromyographic activity and MTU length changes were also measured and compared against the corresponding data predicted by the model. Model-predicted muscle forces, activation levels, and MTU length changes were consistent with the corresponding quantities obtained from experiment. The calculated values of muscle force obtained from static optimization agreed more closely with experiment than those derived from CMC.
[DOI: 10.1115/1.4045660]

Keywords: musculoskeletal model, cat hindlimb, static optimization, computed muscle control, muscle force, gait

Introduction

While there is evidence that humans may minimize metabolic cost when walking at their preferred speeds [1–4], how the nervous system selects a specific muscle activation pattern among the infinite number of possibilities that can produce the same movement remains largely unknown for most locomotor tasks. Solving the muscle-force-sharing (redundancy) problem may provide a better understanding of the strategies used by the central nervous system to coordinate motion of the joints during complex tasks like walking. The muscle force-joint torque redundancy problem reflects the fact that for many musculoskeletal systems in nature, the number of muscles crossing a joint exceeds the number of degrees-of-freedom (DOF) defining joint motion [5–9]. A recent study proposed a novel noninvasive approach for the measurement of superficial tendon loading [10], however, direct measurement of muscle force remains highly invasive and very few studies have recorded muscle or tendon forces in living people. Ates et al. [11,12] measured the forces developed by the individual leg muscles of living people, but these data were recorded intraoperatively and do not reflect the muscle activation patterns adopted during daily physical activity. Komi and colleagues used a buckle transducer to record forces transmitted to the Achilles tendon during human gait [13,14]; however, this approach is ethically questionable and cannot easily be repeated.

Computational modeling offers a feasible alternative for determining muscle forces in vivo. This approach has been used to calculate individual muscle forces [15] and articular contact stress distributions [16], quantify joint function [17,18], and investigate joint stability and injury mechanisms [19]. Musculoskeletal modeling also has been used to simulate the effects of surgeries [20,21], diagnose the causes of abnormal gait [22,23], infer the functional roles of muscles during gait [24–27], investigate neuromuscular coordination [28], analyze sport movements [29], and compute bone-to-bone contact forces at a joint [30].

Importantly, however, the accuracy of model-predicted muscle forces remains largely unknown. Some studies have compared model calculations of muscle force against muscle electromyography (EMG) activity measured for a wide variety of locomotor conditions [28,31,32]. While EMG measurements provide quantitative information on the sequence and timing of muscle activity, there are a number of factors that limit its use in validating predictions of muscle force, including the highly nonlinear and nonunique relationship between EMG and force, and the dependence of this relationship on the length of the muscle, the velocity of shortening or lengthening, the history of contraction, fatigue, and training versus detraining effects [33]. Rigorous validation of muscle force calculations requires a quantitative comparison of

[1]Corresponding author.

Manuscript received March 27, 2019; final manuscript received November 8, 2019; published online February 19, 2020. Assoc. Editor: Brittany Coats.

model-predicted muscle forces against direct measurements of the same quantities obtained for as many muscles as possible and a wide range of movement conditions.

OPENSIM, an open-source musculoskeletal modeling and simulation environment, allows individual muscle forces to be calculated using both inverse- and forward-dynamics techniques [34]. In the inverse-dynamics approach, a physiologically based cost function is optimized at each time instant using static optimization (SO) and the resultant joint moments are considered as constraints needed to satisfy the moment equilibrium regardless of the previous history of force developed by a muscle [35]. Although computationally efficient, this approach does not account for the time-dependent and transient properties of skeletal muscle contraction dynamics [36,37]. Forward-dynamics methods such as computed muscle control (CMC) [38] solve the muscle redundancy problem by exploiting feedback control theory to generate a set of muscle excitations that track a set of desired joint motions [31]. CMC combines forward integration of the dynamical equations of motion with SO to calculate individual muscle forces, and hence, accounts for the time-dependent and transient dynamical behavior of muscle. In contrast to SO, CMC incorporates passive forces in muscle force calculations. Lin et al. [31] compared muscle force predictions derived from SO and CMC for human walking and running and found that both techniques produced similar results, but the authors recommended the use of SO based on its robustness and computational efficiency.

Because in vivo human muscle force recordings are ethically questionable, animal models provide a good starting point for direct validation of muscle forces predicted by computational simulation platforms. Thus, the aim of this study was threefold: first, to develop a detailed musculoskeletal model of the cat hindlimb; second, to apply SO and CMC and determine individual muscle forces in the cat hindlimb during free locomotion, specifically, walking on level ground and walking up inclines of various grades; and third, to quantitatively compare model-predicted muscle forces against direct measurements of the same quantities obtained in vivo during gait.

Materials and Methods

Experimental Protocol. Biomechanical measurements were performed on the cat hindlimb for a wide range of locomotor conditions [39]. Five male cats (5.2 ± 1.1 kg) were trained to walk on level ground and uphill at three different inclines (30 deg, 45 deg, and 60 deg). Training sessions were conducted five times a week for about 1 h for a minimum of 2 months prior to surgical implantation of tendon force transducers and EMG electrodes. Measurements were conducted 1 week following surgery, which allowed for complete recovery of the gait patterns for all animals such that the recorded kinematics and kinetics data after surgery were similar to those observed prior to surgery [40]. All procedures were approved by the Life Sciences Animal Ethics Committee of the University of Calgary.

A prophylactic dose of penicillin-based antibiotic (200,000 I.U. Derapeu-C, Ayerst Labs, Wayne, PA) was administered to the cats. The animals were given a tranquilizer (Atravet 0.5 mg kg^{-1}, Ayerst Labs, Wayne, PA) on the morning of surgery, anesthetized using a halothane-oxygen-nitrous oxide mixture, and then intubated.

Forces transmitted by the medial gastrocnemius (MG), soleus (SOL), and tibialis anterior (TA) tendons in the left hindlimb were measured using buckle transducers (Fig. 1) [41]. Each transducer was surgically attached to the separated tendon of the respective muscle, and muscle force was recorded at 2000 Hz [42]. Tendon force transducers were based on the design of Walmsley et al. [43]. Stainless steel (316 alloy) was fashioned into smooth E-shaped pieces. A small hole was drilled into the ends of the arms of the E to allow for the placement of sutures on the open end of the E following attachment of the transducer on the tendon.

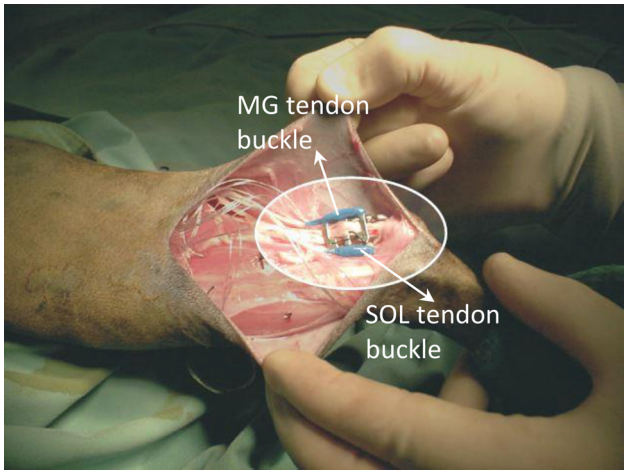

Fig. 1 Buckle-type force transducers attached to the MG and SOL muscle tendons in the cat hindlimb

This design prevented the transducer from slipping over the tendon. The tendon force transducers were calibrated at the end of the measurement session. Once the animals were anesthetized, transducers were calibrated by detaching the insertion areas of the muscle-tendon units (MTUs) from the attached bone and hanging a series of at least 15 known weights from the remnant tendon. Calibrations of each transducer turned out to be linear within the physiologic loading range with a linear regression coefficient typically exceeding 0.99 [40].

Muscle EMG activity for the MG, SOL, and TA was measured using in-dwelling, bipolar, fine-wire electrodes sampling at 2000 Hz. The in-dwelling bipolar EMG electrodes were composed of Teflon-insulated multistranded, stainless steel wire (Bergen BW9-48) and were surgically implanted into the midbelly of the target muscles using a small, curved surgeon's needle (Miltex

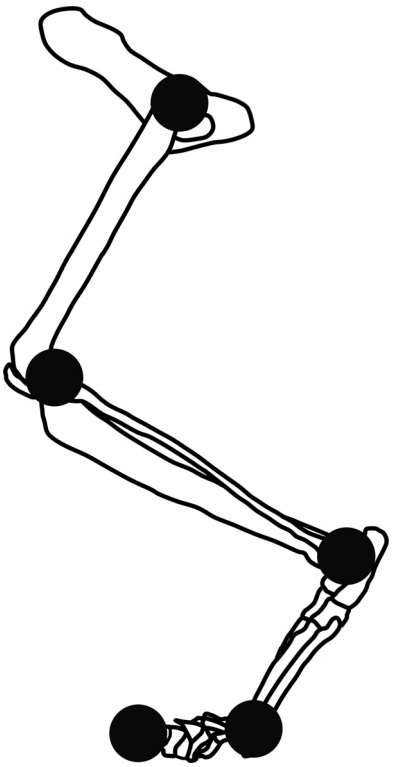

Fig. 2 Placement sites of the reflective markers on the cat hindlimb

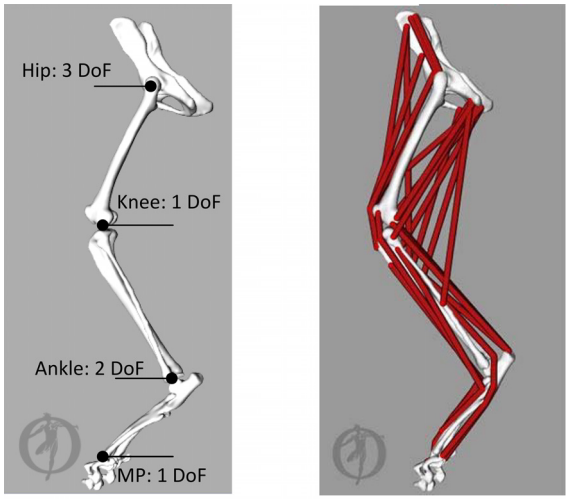

Fig. 3 (*a*) Skeletal and (*b*) musculoskeletal models of the cat hindlimb used in this study. DOF: degrees-of-freedom; MP: metatarsophalangeal joint.

MS-140). The EMG electrodes were fixed to the muscular fascia using silk sutures [40]. Leads of all EMG electrodes and force transducers were routed subcutaneously to a backpack connector from which all signals were transmitted by telemetry to a custom-built amplifier. Linear envelopes of the EMG signals were calculated from the full-wave rectified signals treated with a second-order Butterworth low-pass filter operating at a cut-off frequency of 7 Hz [44].

Joint motion of the left hindlimb was measured using five reflective markers, each 10 mm in diameter, placed over the hip, knee, ankle, metatarsophalangeal (MP) joint, and toe (Fig. 2). The three-dimensional spatial positions of these markers were measured using a two-camera motion capture system (DRMC36, Motion Analysis Corporation, Santa Rosa, CA) sampling at 60 Hz. The three-dimensional position of the contralateral hip joint marker was chosen to be roughly symmetric with the position of the ipsilateral hip joint marker. Cats walked on the walkway at self-selected speed (average speeds were 0.39 ± 0.11 m/s, 0.65 ± 0.17 m/s, 0.76 ± 0.15 m/s, and 0.85 ± 0.20 m/s for the level and the 30 deg, 45 deg, and 60 deg uphill walking conditions, respectively).

Muscle-tendon lengths of the MG, SOL, and TA were calculated using the measured joint motion and corresponding moment arms. Muscle-tendon moment arms were determined as a function of joint angle using the tendon excursion method [39,45].

Left hindlimb ground reaction forces were recorded using two force platforms (AMTI, Newton, MA) positioned in the center of the walkway. Ground reaction forces were recorded at 2000 Hz and synchronized with the kinematic, muscle force, and EMG data. Paw contact was identified as the first instant at which the vertical component of the ground reaction force was greater than 5% of bodyweight. Similarly, paw-off was identified as the first instant at which the vertical component of the ground reaction force was less than 5% of body weight. For more details concerning the surgical and experimental procedures, see Herzog et al. [40].

Musculoskeletal Model of the Cat Hindlimb. A rigid-body model of the hindlimb skeleton was created in OPENSIM (version 3.3) using computed tomography (CT) images with slice thickness of 0.075 cm and voxel size of $0.05 \times 0.05 \times 0.075\ \text{cm}^3$ (Siemens Emotion 16, Erlangen, Germany) obtained from one male adult cat. The two-dimensional CT images were converted into a three-dimensional model using a commercial image processing software package called 3D DOCTOR (Able Software Corp., Lexington, MA).

Table 1 Peak knee and ankle moment arms measured and computed for the cat hindlimb

	Moment arms obtained with OPENSIM		Moment arms given in the literature	
Muscle	Knee flexion (mm)	Ankle flexion (mm)	Knee flexion[a] (mm)	Ankle flexion[b] (mm)
BFM	−9.3	—	−10.1	—
BFP	−61	—	−62.0	—
EDL	3.0	11.4	2.7	12.3
FHL	—	−5.9	—	−5.7
GRA	−28.6	—	−28.2	—
LG	−9.2	−14.9	−8.8	−16.0
MG	−9.2	−14.9	−8.6	−16.0
PL	—	3.4	—	3.7
PLAN	−9.2	−15.0	−9.4	−16.0
RF	10.6	—	10.5	—
SM	−6.3	—	−6.7	—
SMP	−11.6	—	−10.0	—
SOL	—	−15.0	—	−16.0
ST	−39.3		−40.0	
TA	—	12.1	—	12.0
VI	9.9	—	9.8	—
VL	9.9	—	9.5	—
VM	10.0	—	9.8	—

[a]Literature values of knee flexion moment arms from Ref. [51].
[b]Literature values of ankle flexion moment arms from Refs. [47] and [50].
Note: The missing values (—) imply that either the corresponding muscle does not span the respective joint or the moment arm value cannot be found in the literature. BFM: biceps femoris medial; BFP: biceps femoris posterior; EDL: extensor digitorum longus; FHL: flexor hallucis longus; GRA: gracilis; LG: lateral gastrocnemius; MG: medial gastrocnemius; PL: peroneus longus; PLAN: plantaris; RF: rectus femoris; SM: semimembranosus; SMP: semimembranosus posterior; SOL: soleus; ST: semitendinosus; TA: tibialis anterior; VI: vastus intermedius; VL: vastus lateralis; VM: vastus medialis.

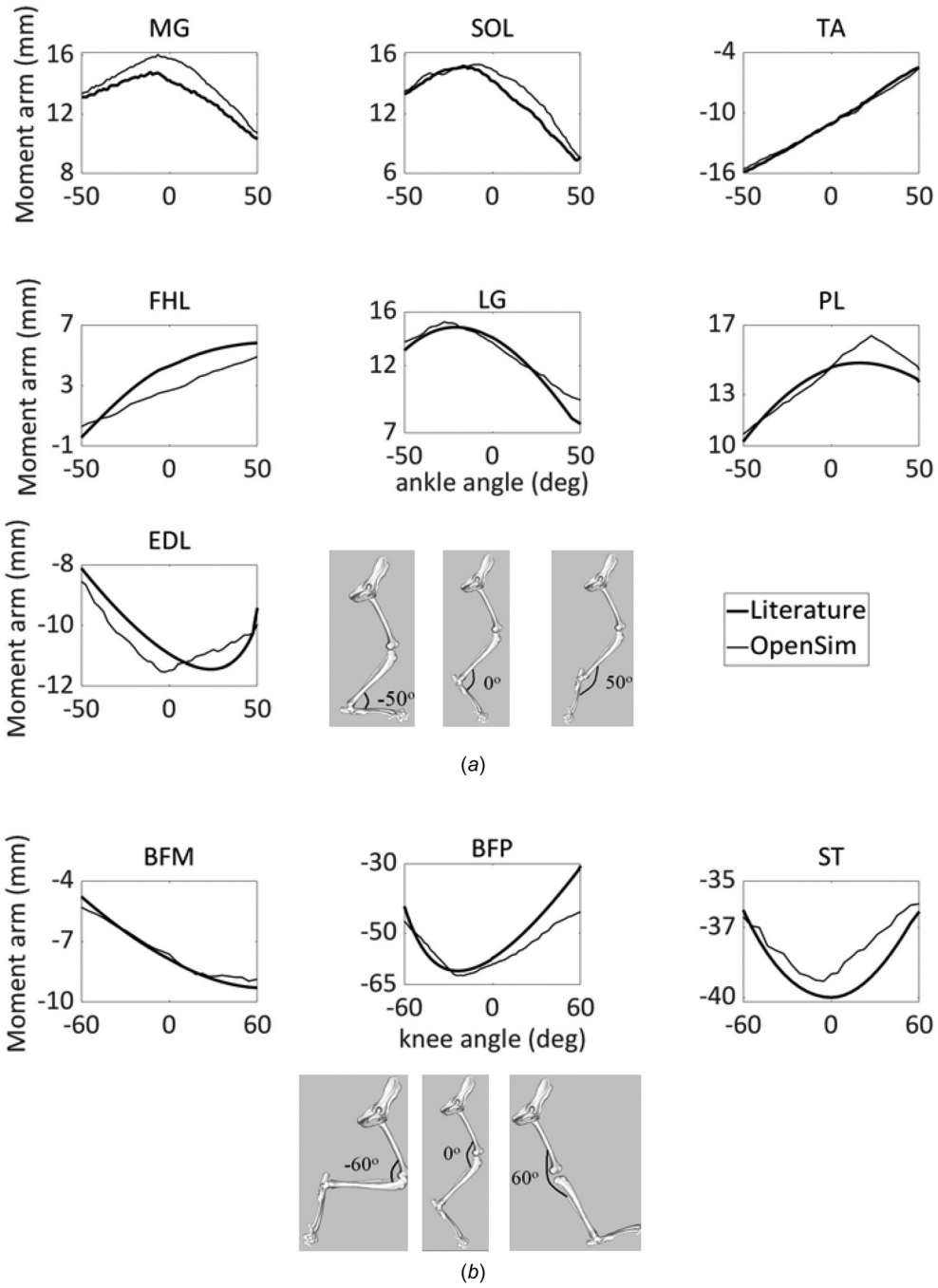

Fig. 4 Comparison of the moment arms as a function of (*a*) ankle joint angle for seven muscles obtained from OPENSIM and literature studies [47,50,51] (MG: medial gastrocnemius; SOL: soleus; TA: tibialis anterior; EDL: extensor digitorum longus; FHL: flexor hallucis longus; LG: lateral gastrocnemius; PL: plantaris) and (*b*) knee joint angle for three muscles (BFM: biceps femoris medial; BFP: biceps femoris posterior; ST: semitendinosus)

Closed mesh surfaces of the bones were then created using SolidWorks (Dassault Systems SolidWorks Corp., Waltham, MA). The inertial parameters (moment of inertia, mass, and center of mass) of each bone were calculated by taking into account the geometry of the bones determined from SolidWorks as well as the density of bone [46]. The model of the cat hindlimb consisted of five rigid bodies—pelvis, thigh, shank, foot, and the digits—and 13DOF (Fig. 3(*a*)). The pelvis was represented as a 6DOF free joint, the hip as a 3DOF ball-and-socket joint, the knee as a 1DOF hinge joint, the ankle as a 2DOF universal joint, and the MP joint as a 1DOF hinge joint (Fig. 3(*a*)). A rotation matrix for each body segment was obtained from the local coordinate system embedded at the center of each joint relative to the global coordinate system. Rotations about the longitudinal axis of the segment (except for the hip joint) were neglected since rotations of each body segment were represented by two markers only. The locations of the axes of rotation for each joint were found using a mechanical system as described by Burkholder and Nichols [47]. Directions of the axes were selected to be consistent with those defined in OPENSIM. Following the determination of axes, a stance-like posture was selected as a reference position for the skeletal system, and all joint angles were set to zero in this neutral pose [47,48]. For the hip and knee joints, the reference position was set at mild flexion. The reference position for the ankle joint was set at mild

Table 2 Muscle model parameter values assumed in this study

Muscle	Abbreviation	Optimal fiber length (mm)	Tendon slack length (mm)	Peak isometric muscle force (N)	Pennation angle (deg)
Adductor magnus	ADDMAG	62.6	31.0	103	0
Biceps femoris anterior	BFA	36.9	81.0	87	14
Biceps femoris medial	BFM	36.9	85.0	61	14
Biceps femoris posterior	BFP	44.3	92.5	22	14
Extensor digitorum longus	EDL	33.6	172.0	22	8
Flexor digitorum longus	FDL	20.6	179.0	21	10
Flexor hallucis longus	FHL	15.6	175.0	110	7
Gluteus medius	GMED	12.0	34.0	60	10
Gluteus minimus	GMIN	10.5	33.6	22	10
Gracilis	GRA	64.4	47.8	31	0
Lateral gastrocnemius	LG	24.5	101.7	105	17
Medial gastrocnemius	MG	20.9	107.5	92	21
Peroneus longus	PL	23.7	107.0	17	7
Plantaris	PLAN	18.7	112.5	78	14
Rectus femoris[a]	RF	19.2	91.5	124	7
Sartorius anterior	SARA	105.5	28.0	8	0
Sartorius medial	SARM	105.5	30.0	12	0
Semimembranosus anterior	SMA	84.0	25.0	39	0
Semimembranosus posterior	SMP	62.0	60.0	79	0
Semitendinosus	ST	60.5	62.5	48	0
Soleus	SOL	41.7	65.0	21	7
Tibalis anterior	TA	52.2	85.9	27	7
Vastus intermedius	VI	22.6	70.0	42	7
Vastus lateralis[a]	VL	27.3	72.0	150	17
Vastus medialis	VM	26.9	65.0	62	17

[a]Indicates that the muscle-tendon parameters were obtained from Ref. [53].
Note: All muscle parameters (except those indicated by footnote a) were obtained from Ref. [52].

dorsiflexion, while that for the MP joint was set at full extension. The model skeleton was actuated by 25 Hill-type muscle-tendon units (Fig. 3(*b*)) [47,49–51]. Muscle origin and insertion sites were determined using published anatomical records [47]. Via points and wrapping surfaces were added to provide an anatomically realistic path for each MTU [48]. The locations of the origin and insertion sites of the MTUs were adjusted until the moment arms computed in the model were in reasonable agreement with the corresponding data reported in the literature [47,50,51] (see Table 1 and Fig. 4).

Physiological parameters for the model of muscle-tendon actuation (i.e., peak isometric muscle force and the corresponding optimal muscle-fiber length and pennation angle as well as tendon slack length) were obtained from the literature (see Table 2) [52,53]. Muscle excitation-contraction (activation) dynamics were modeled as a first-order process with activation and deactivation time constants assumed to be 10 ms and 40 ms, respectively [54].

Muscle Force Calculations. The generic skeletal model was scaled to each cat such that the distances between the locations of the experimental and virtual (theoretical) markers were minimized. Joint angles were calculated from the marker data by means of an inverse kinematics approach [34]. A standard inverse-dynamics approach was used to compute the net moments exerted about the hindlimb MP, ankle, knee, and hip joints [28]. SO and CMC were then used to determine the individual muscle forces at each instant during the gait cycle. The fast target CMC algorithm was implemented in this study. The objective function was to minimize the sum of the squares of all muscle activations subject to the force–length and force–velocity properties of the muscles [55]. Length changes of the muscle-tendon units were found using the "Muscle Analysis" tool available in OPENSIM.

Data Analysis. Only the results for the stance phase of locomotion are presented below because the muscles of interest, MG and SOL, remain primarily active during this phase. To quantitatively evaluate the agreement between model and experiment, root-mean-square differences (RMSDs) and Pearson cross-correlation coefficients (PCCs) were calculated for measured and model-predicted muscle forces, MTU length changes, and muscle activations. An RMSD value of 0.01 indicates a mean error of 1% between the measured and model-predicted data, while a PCC value of 0 indicates no correlation between the measured and model-predicted results [56]. Differences in RMSD and PCC values between the measured and model-predicted muscle forces and muscle activations were evaluated statistically using a multiway analysis of variance. Holm–Bonferroni correction was used for multiple comparisons. The level of significance was set to $p < 0.05$.

Model Sensitivity Analysis. Monte Carlo analyses were used to quantify the sensitivity of the model-predicted muscle forces to combined changes in five physiological parameters of each MTU: peak isometric muscle force, optimal muscle fiber length, muscle pennation angle, tendon slack length, and maximum contraction velocity of muscle [57]. The model-predicted muscle forces obtained from the generic model for all locomotion conditions served as the nominal muscle forces. For each MTU, the SO and CMC problems were resolved by randomly perturbing each

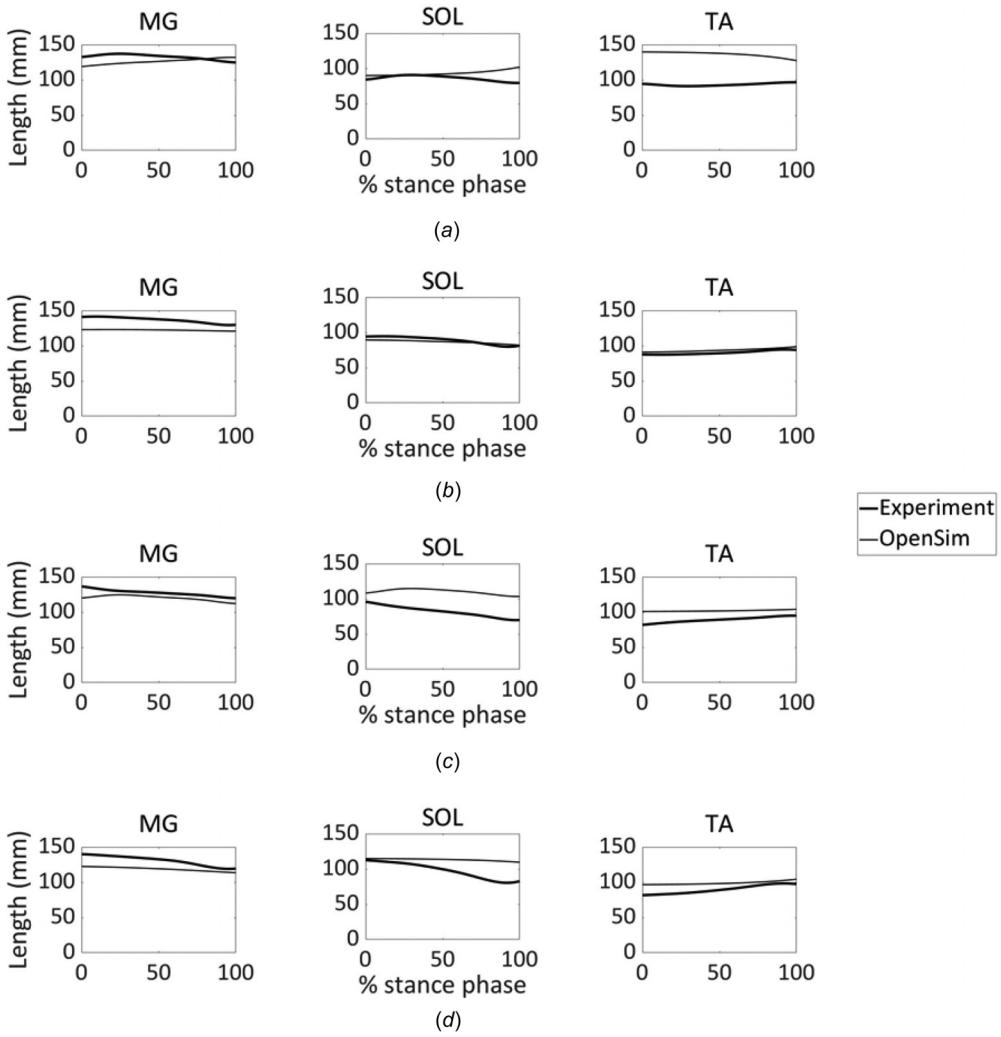

Fig. 5 Comparison between the measured and model-predicted muscle-tendon unit lengths for the MG, SOL, and TA muscles in the cat hindlimb during (*a*) level walking, (*b*) walking up a 30 deg incline, (*c*) walking up a 45 deg incline, and (*d*) walking up a 60 deg incline. Data were normalized to the stance phases of each stride.

Table 3 Average RMSD and PCC values for muscle-tendon unit length changes obtained experimentally and predicted theoretically for different locomotion conditions

	Level walking			30 deg upslope			45 deg upslope			60 deg upslope		
	MG	SOL	TA	MG	SOL	TA	MG	SOL	TA	MG	SOL	TA
RMSD	0.07	0.11	0.46	0.11	0.04	0.04	0.06	0.35	0.15	0.10	0.19	0.11
PCC	0.82	0.85	0.79	0.95	0.98	0.98	0.86	0.73	0.94	0.93	0.84	0.91

physiological parameter between +10% and −10% of its nominal value. For each new solution, a RMSD was calculated reflecting the difference between the model-predicted muscle force associated with the perturbed physiological parameter and that associated with the nominal solution. For each Monte Carlo simulation, a convergence criterion was defined as a stopping rule [58]. The criterion was satisfied when the mean and the coefficient of variation for the final 10% of the simulations were within 2% of the entire mean and coefficient of variation [57].

Results

Muscle-tendon unit length changes calculated for MG, SOL, and TA were consistent with those obtained from experiment (Fig. 5). RMSD between the calculated and measured MTU length changes were less than 0.20 for all three muscles and locomotion conditions, except for TA during level walking and SOL when walking up a 45 deg incline (Table 3). The corresponding mean PCC values were at least 0.73 across all muscles and locomotion conditions (Table 3).

The activation patterns predicted by both SO and CMC were generally consistent with the measured EMG data (Fig. 6), except for TA and MG when walking up the 45 deg and 60 deg inclines, respectively, where relatively high RMSD values and low correlation coefficients were observed (Fig. 7).

Muscle forces predicted by SO agreed more closely with experiment than those derived from CMC (Fig. 8). RMSD values

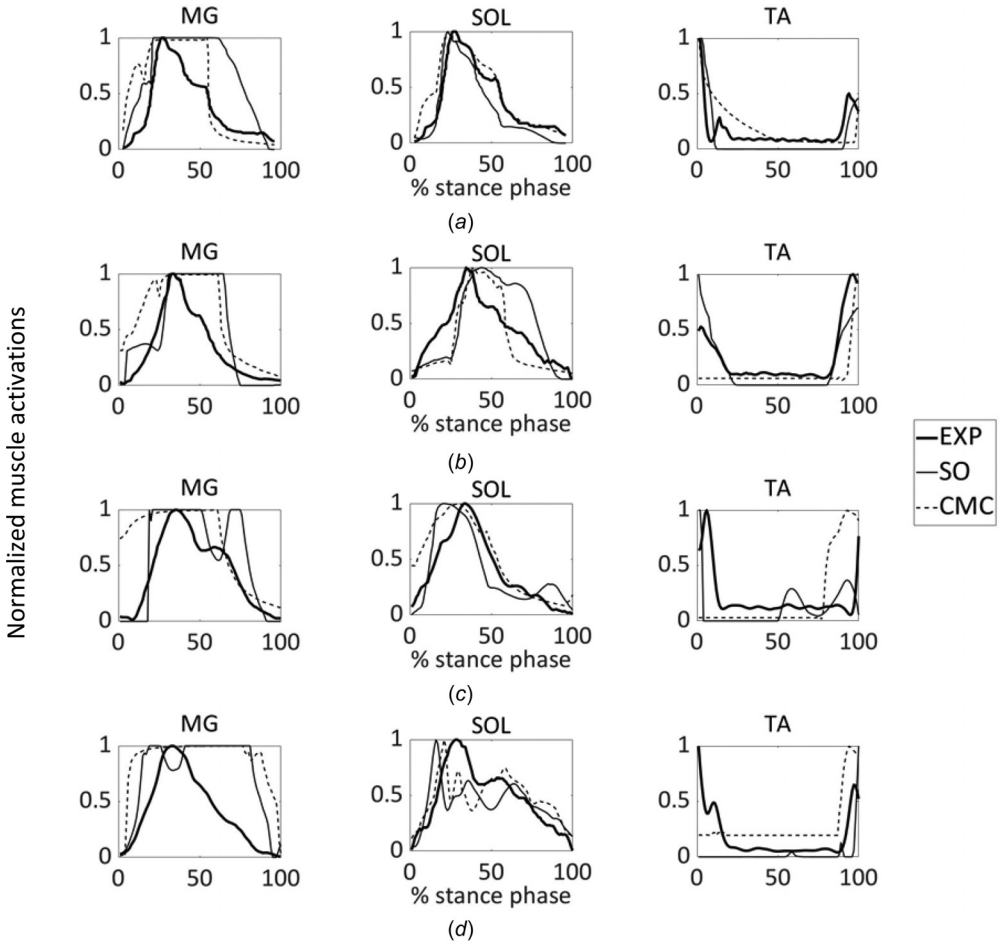

Fig. 6 Comparison between the measured and model-predicted activation patterns for the MG, SOL, and TA muscles in the cat hindlimb for (*a*) level walking, (*b*) walking up a 30 deg incline, (*c*) walking up a 45 deg incline, and (*d*) walking up a 60 deg incline. Data were normalized to the stance phase of each stride. Magnitudes of the measured and model-predicted activation patterns were normalized from 0 to 1 based upon the minimum and maximum values obtained during stance. EXP: linear envelope of the measured EMG signal normalized to its peak value; SO: muscle activation predicted by static optimization; CMC: muscle activation predicted by computed muscle control.

for SO were consistently smaller than those for CMC for all muscles and all locomotion conditions (Fig. 9). Except for SOL in level walking and TA when walking up a 60 deg incline, muscle force predictions obtained using SO were associated with a significantly smaller error than those obtained from CMC ($p < 0.05$). PCC analysis also showed that the level of agreement between the model-predicted and measured muscle forces was greater for SO than CMC; however, a statistically significant difference ($p < 0.05$) was detected only for MG during level walking (Fig. 9).

The sensitivity analyses revealed that mean RMSD values calculated between the model-predicted nominal muscle forces and the muscle forces obtained from Monte Carlo analyses using SO were consistently smaller than those obtained using CMC for all muscles and all locomotion conditions (Figs. 10 and 11, Table 4). The sensitivity results of the PCC analysis also demonstrated that mean PCC values calculated between the model-predicted nominal muscle forces and the muscle forces obtained from Monte Carlo analyses using SO were greater than those obtained from CMC for all muscles and locomotion conditions (Table 5).

In all simulations, peak reserve joint moments were less than 5% of the corresponding net joint moment. Peak reserve joint moments for CMC were greater than those for SO, except for the 30 deg uphill walking ($p < 0.05$). Residual joint moments were less than 1% BW × Ht, while residual forces were less than 5% of the magnitude of the vertical ground reaction force as recommended by Hicks et al. [59].

Discussion

Accurate determination of the force-sharing patterns among muscles during unrestrained voluntary movements remains a challenging problem in biomechanics [60,61]. Computational modeling is the only practical means of evaluating muscle and joint contact loading in vivo. However, one limitation of the existing models is the lack of systematic and objective validation of the predicted muscle forces [59]. The purpose of this study was to quantitatively evaluate the accuracy of model-predicted muscle forces derived from two of the most widely used optimization-based techniques in the study of human motion biomechanics—SO and CMC—against direct measurements of the same quantities obtained in vivo. Muscle forces were calculated using a muscle-actuated model of the cat hindlimb in conjunction with the experimental gait data obtained for level walking and walking up inclined surfaces. There was good agreement between the calculated and measured MTU length changes, and hence muscle-tendon moment arms, implying that the geometry of the muscles and bones assumed in the model was reasonable (Fig. 5, Table 3). The calculated values of MG, SOL, and TA forces obtained from SO were compared more favorably with experiment than those

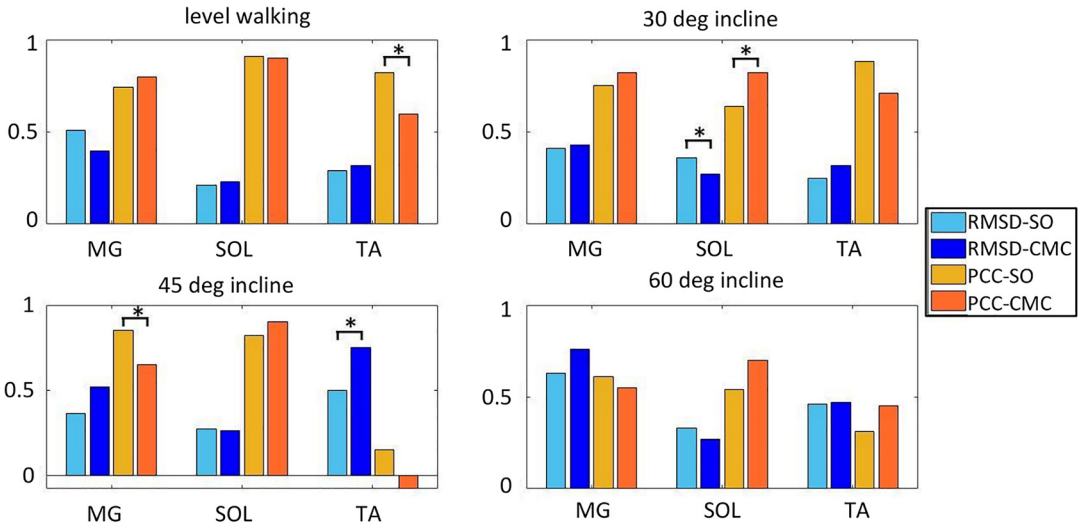

Fig. 7 Average RMSD and PCC values reflecting differences between the measured and model-predicted muscle activation patterns obtained from SO and CMC for different locomotion conditions (MG: medial gastrocnemius; SOL: soleus; TA: tibialis anterior). * indicates statistical difference between SO and CMC ($p < 0.05$).

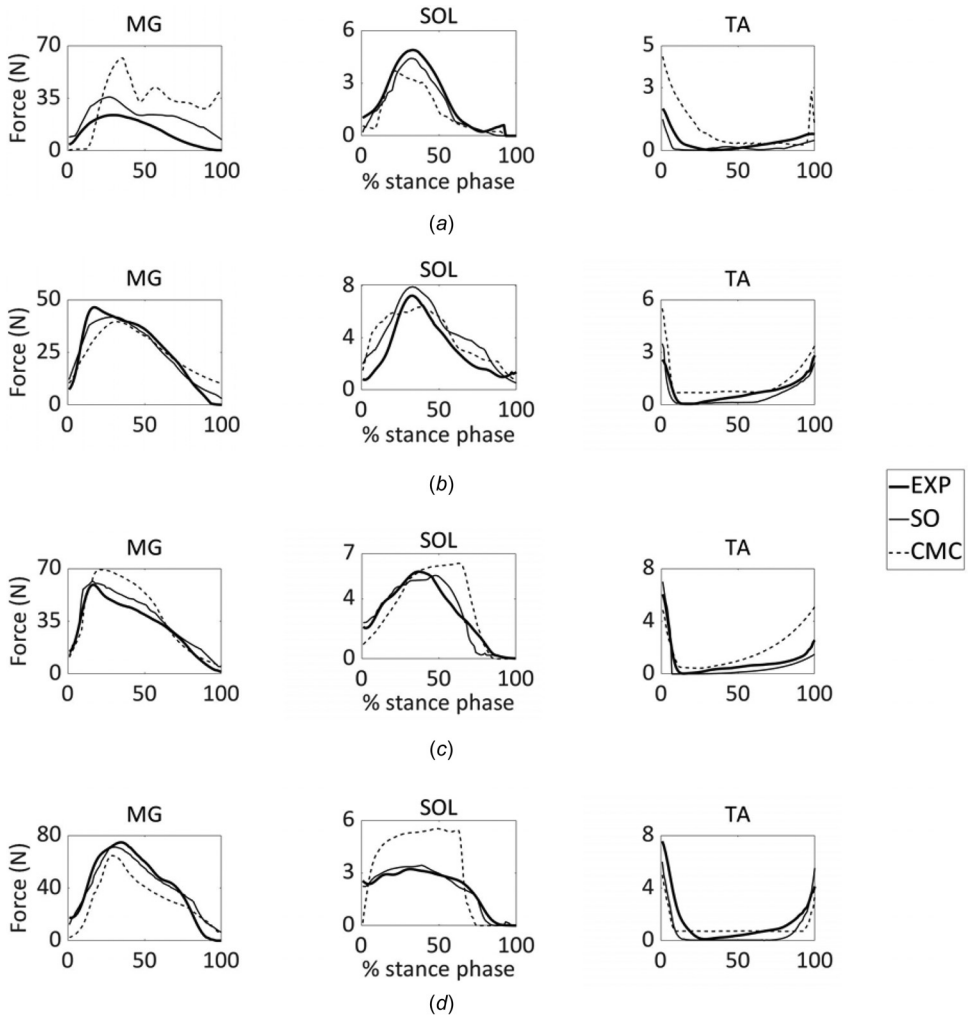

Fig. 8 Comparison between the measured and model-predicted forces for the MG, SOL, and TA muscles in the cat hindlimb during (*a*) level walking, (*b*) walking up a 30 deg incline, (*c*) walking up a 45 deg incline, and (*d*) walking up a 60 deg incline. Data were normalized to the stance phase of each stride. EXP: measured muscle force; SO: muscle force predicted by static optimization; CMC: muscle force predicted by computed muscle control.

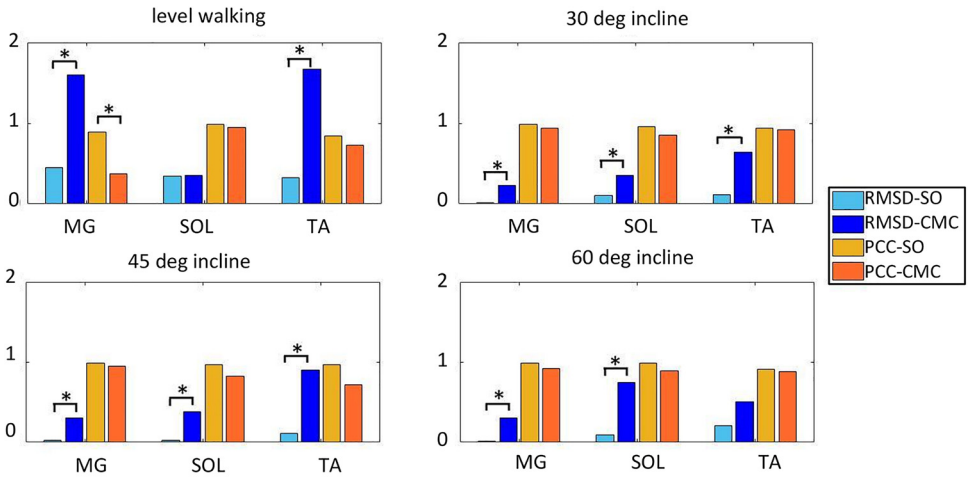

Fig. 9 Average RMSD and PCC values reflecting differences between the measured and model-predicted muscle forces obtained from SO and CMC for different locomotion conditions (MG: medial gastrocnemius; SOL: soleus; TA: tibialis anterior). * indicates statistical difference between SO and CMC for the corresponding muscle ($p < 0.05$).

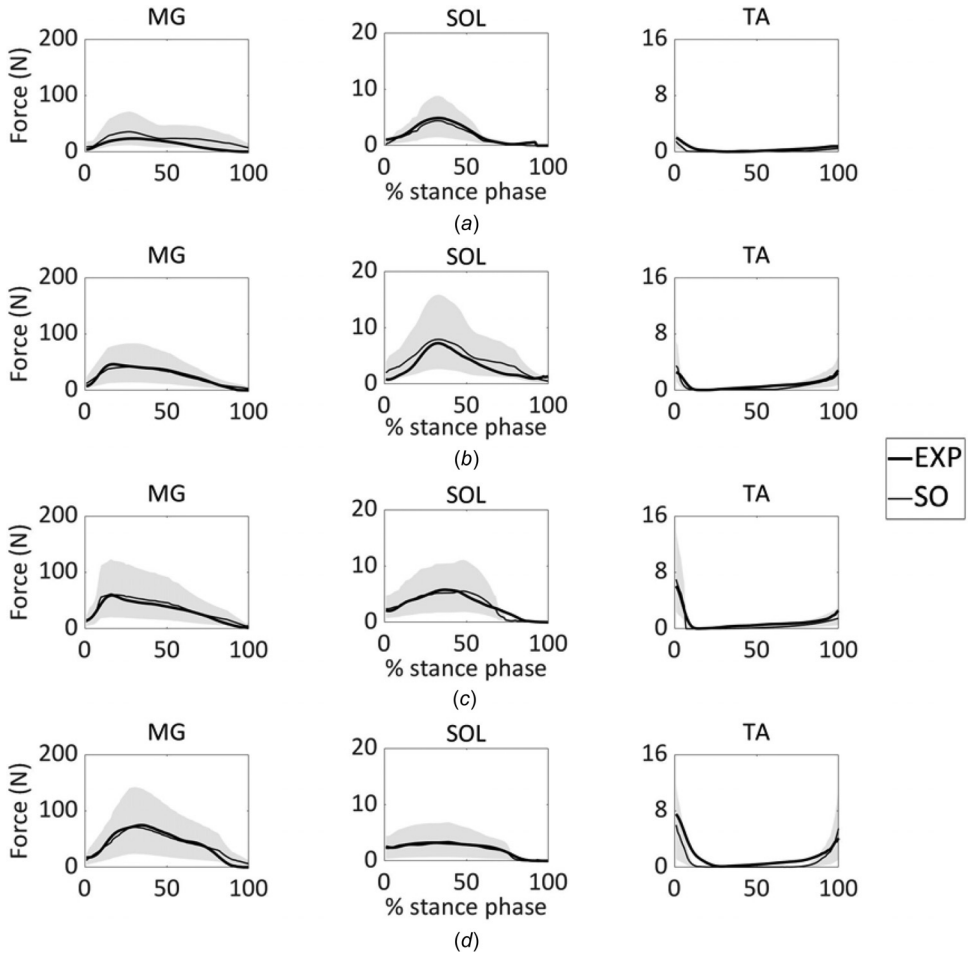

Fig. 10 Variations in muscle forces obtained from Monte Carlo analyses (gray shaded regions) together with measured (thick lines) and model-predicted forces (thin lines) for the MG, SOL, and TA muscles in the cat hindlimb during (*a*) level walking, (*b*) walking up a 30 deg incline, (*c*) walking up a 45 deg incline, and (*d*) walking up a 60 deg incline. Data were normalized to the stance phase of each stride. Model-predicted muscle forces were calculated using static optimization simulations where peak isometric muscle force, optimal muscle fiber length, muscle pennation angle, tendon slack length, and maximum contraction velocity of muscle for each muscle-tendon unit were varied simultaneously. EXP: measured muscle force; SO: muscle force calculated using static optimization.

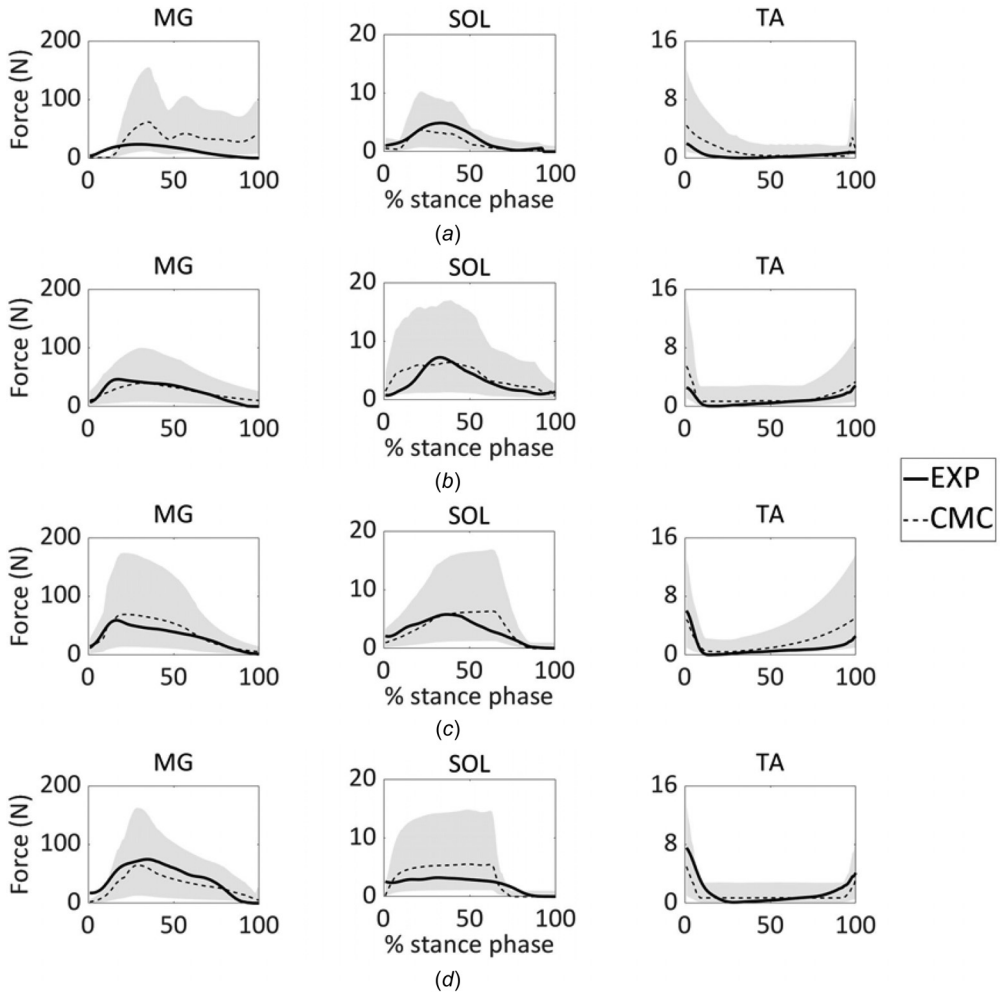

Fig. 11 Variations in muscle forces obtained from Monte Carlo analyses (gray shaded regions) together with measured (thick lines) and model-predicted forces (thin lines) for the MG, SOL, and TA muscles in the cat hindlimb during (*a*) level walking, (*b*) walking up a 30 deg incline, (*c*) walking up a 45 deg incline, and (*d*) walking up a 60 deg incline. Data were normalized to the stance phase of each stride. Model-predicted muscle forces were calculated using computed muscle control simulations where peak isometric muscle force, optimal muscle fiber length, muscle pennation angle, tendon slack length, and maximum contraction velocity of muscle for each muscle-tendon unit were varied simultaneously. EXP: measured muscle force; CMC: muscle force calculated using computed muscle control.

predicted by CMC (Figs. 8 and 9), supporting the use of this method as a tool for predicting muscle forces during gait [31]. RMSD values between the measured and model-predicted forces for SO were smaller than those obtained by CMC for all muscles and all locomotion conditions (Fig. 9). PCC analysis also showed that the level of agreement between the model-predicted and measured muscle forces was greater for SO than CMC (Fig. 9).

One possible explanation for the differences in the model-predicted muscle forces between SO and CMC is the inclusion of passive muscle forces in CMC [62,63]; in particular, the SO algorithm ignores the passive force generated by muscle's parallel elastic element. To investigate the contribution of passive muscle forces in the CMC results, we partitioned the total muscle force into active and passive muscle forces for MG, SOL, and TA during all locomotion conditions (Table 6). In some cases, passive muscle forces contributed excessively to the total forces obtained from CMC, especially for the cases of MG and TA during level walking, indicating that the disagreement between the measured and model-predicted muscle forces may be partially attributed to the calculation of the passive muscle forces.

Muscle force estimates obtained from SO were less sensitive to changes in the values assumed for the muscle-tendon parameters than those derived from CMC (Tables 4 and 5). This result may be explained by the fact that the SO method implemented in OPENSIM 3.3 ignores the effects of tendon compliance, whereas the calculated values of muscle forces are known to be particularly sensitive to changes in tendon slack length, and hence, tendon compliance [57].

There are a number of limitations of this study that must be considered when interpreting the results. First, contractile forces were measured for only three muscles because of the technical challenges involved in obtaining these measurements in vivo. Second, the experimental gait data and model geometry were derived from different animals. Ideally, the experimental and modeling work would be performed on the same animal, but this was not possible here as the cadaver limbs of the animals on which the experiments were performed were not available post hoc. Third, the skeletal model of the cat hindlimb was based on CT scans from a single cat. Although we implemented a scaling procedure to account for different sizes of animals used in the experiments, the scaling may not accurately reflect all of the anatomical differences present. Fourth, the patella was assumed to remain fixed relative to the femur. Even though we focused on the ankle muscles in this study, immobilization of the patella may affect the

Table 4 Average RMSD values reflecting differences between the nominal and perturbed muscle forces obtained from Monte Carlo analyses using SO and CMC for different locomotion conditions

		Level walking			30 deg upslope			45 deg upslope			60 deg upslope		
		MG[a]	SOL	TA[a]	MG	SOL[a]	TA[a]	MG[a]	SOL[a]	TA[a]	MG	SOL[a]	TA
SO	Mean	0.98	0.29	0.45	0.55	0.62	0.36	0.55	0.42	0.52	0.47	0.42	0.29
	Max	1.58	0.69	0.78	0.80	1.11	0.78	1.15	0.94	0.93	0.89	0.92	0.81
	Min	0.01	0.0	0.08	0.0	0.0	0.01	0.04	0.01	0.0	0.0	0.01	0.01
CMC	Mean	2.98	0.38	2.25	0.78	0.98	1.45	0.98	1.22	1.78	0.52	1.45	0.42
	Max	4.25	0.98	4.45	1.11	1.98	2.87	1.89	1.78	3.11	0.85	2.95	0.89
	Min	0.15	0.01	0.09	0.01	0.02	0.08	0.02	0.01	0.0	0.0	0.02	0.01

[a]Indicates statistical difference between SO and CMC for the corresponding muscle ($p < 0.05$).
Note: Max and Min represent the maximum and minimum RMSD values, respectively.

Table 5 Average PCC values reflecting differences between the nominal and perturbed muscle forces obtained from Monte Carlo analyses using SO and CMC for different locomotion conditions

		Level walking			30 deg upslope			45 deg upslope			60 deg upslope		
		MG[a]	SOL[a]	TA[a]	MG[a]	SOL[a]	TA[a]	MG	SOL[a]	TA[a]	MG[a]	SOL[a]	TA[a]
SO	Mean	0.95	0.97	0.92	0.97	0.93	0.95	0.91	0.98	0.95	0.97	0.95	0.92
	Max	0.96	0.98	0.97	0.98	0.97	0.98	0.95	0.99	0.97	0.98	0.98	0.95
	Min	0.87	0.85	0.85	0.86	0.85	0.89	0.88	0.85	0.89	0.91	0.91	0.89
CMC	Mean	0.65	0.85	0.62	0.85	0.75	0.88	0.82	0.76	0.66	0.78	0.74	0.75
	Max	0.71	0.89	0.72	0.90	0.88	0.91	0.89	0.83	0.75	0.87	0.81	0.81
	Min	0.55	0.62	0.55	0.72	0.70	0.75	0.78	0.68	0.56	0.69	0.66	0.69

[a]Indicates statistical difference between SO and CMC for the corresponding muscle ($p < 0.05$).
Note: Max and Min represent the maximum and minimum PCC values, respectively.

Table 6 Average RMSD and PCC values reflecting differences between the measured and model-predicted muscle forces obtained from CMC for different locomotion conditions (MG: medial gastrocnemius; SOL: soleus; TA: tibialis anterior)

	Level walking			30 deg upslope			45 deg upslope			60 deg upslope		
	MG	SOL	TA	MG	SOL	TA	MG	SOL	TA	MG	SOL	TA
RMSD												
CMC	1.60	0.35	1.67	0.23	0.35	0.64	0.30	0.38	0.90	0.30	0.75	0.51
CMC-active	0.69	0.35	0.78	0.23	0.35	0.64	0.24	0.29	0.90	0.30	0.37	0.51
PCC												
CMC	0.37	0.95	0.73	0.94	0.85	0.92	0.95	0.83	0.72	0.92	0.89	0.88
CMC-active	0.74	0.95	0.81	0.94	0.85	0.92	0.96	0.88	0.72	0.92	0.90	0.88

Note: CMC-active represents the average RMSD and PCC values reflecting differences between the measured and model-predicted active muscle forces (without passive forces) obtained from CMC.

accuracy of the muscle force predictions obtained using both methods. Finally, generic values of peak isometric muscle force and maximum shortening velocity of muscle were assumed in the model, which may have introduced additional sources of error in the model calculations. However, previous studies have shown that estimates of muscle force are more sensitive to changes in tendon slack length and optimum muscle fiber length than peak isometric force [57,64]. Furthermore, since the experiments were restricted to walking at the normal speed, one would not expect the calculated values of muscle force to be overly sensitive to changes in the value assumed for muscle's intrinsic maximum shortening velocity.

In summary, we found model-predicted muscle forces, activation levels, and MTU length changes to be consistent with experiment for normal locomotion in the cat hindlimb, with the calculated values of muscle force obtained from SO agreeing more closely with measured muscle forces than those derived from CMC. Future work should focus on obtaining in vivo measurements of muscle force for a larger number of animals, different species, and a wide range of motor tasks in the interests of generating a larger corridor of data for model validation.

The musculoskeletal model of the cat hindlimb is freely available online.[2]

Acknowledgment

We thank Professor Motoshi Kaya (The University of Tokyo) for his assistance with collecting and processing the gait data and Professor Chris Whitton (University of Melbourne) for providing the CT images of the cat hindlimb.

Funding Data

- Natural Sciences and Engineering Research Council (NSERC) of Canada; Funder ID: 10.13039/501100002790.

[2]https://simtk.org/home/cat-hindlimb

- The Canada Research Chair Program, The Killam Foundation.
- The Research Fund of Istanbul University (Project no: FDK-2016-21712).
- Scientific and Technological Research Council of Turkey (TUBITAK).
- Australian Research Council (Discovery Project DP160104366).

Nomenclature

BFM = biceps femoris medial
BFP = biceps femoris posterior
BW = body weight
CMC = computed muscle control
CT = computed tomography
DOF = degrees-of-freedom
EDL = extensor digitorum longus
EMG = electromyography
FHL = flexor hallucis longus
GRA = gracilis
Ht = center of mass height
LG = lateral gastrocnemius
MG = medial gastrocnemius
MP = metatarsophalangeal joint
MTU = muscle-tendon unit
PCC = Pearson cross-correlation coefficient
PL = peroneus longus
PLAN = plantaris
RF = rectus femoris
RMSD = root-mean-square difference
SM = semimembranosus
SMP = semimembranosus posterior
SO = static optimization
SOL = soleus
ST = semitendinosus
TA = tibialis anterior
VI = Vastus intermedius
VL = Vastus lateralis
VM = Vastus medialis

Appendix

Moment of inertia and mass values assigned for the skeletal model of the cat hindlimb are given in Table 7.

Table 7 Moment of inertia and mass values assigned for the skeletal model of the cat hindlimb

	Moment of inertia (kg m^2)			
Body	About the anteriorposterior axis	About the longitudinal axis	About the mediolateral axis	Mass (kg)
Pelvis	0.068	0.062	0.041	0.82
Thigh	0.091	0.023	0.033	0.65
Shank	0.035	0.004	0.036	0.26
Foot	0.001	0.003	0.003	0.087
Digits	0.0001	0.0001	0.0007	0.015

References

[1] Anderson, F. C., and Pandy, M. G., 2001, "Dynamic Optimization of Human Walking," ASME J. Biomech. Eng., **123**(5), pp. 381–390.
[2] Donelan, J. M., Kram, R., and Arthur, D. K., 2001, "Mechanical and Metabolic Determinants of the Preferred Step Width in Human Walking," Proc. R. Soc. London B, **268**(1480), pp. 1985–1992.
[3] Collins, S. H., Wiggin, M. B., and Sawicki, G. S., 2015, "Reducing the Energy Cost of Human Walking Using an Unpowered Exoskeleton," Nature, **522**(7555), pp. 212–215.
[4] Shorter, K. A., Wu, A., and Kuo, A. D., 2017, "The High Cost of Swing Leg Circumduction During Human Walking," Gait Posture, **54**, pp. 265–270.
[5] Crowninshield, R. D., and Brand, R. A., 1981, "The Prediction of Forces in Joint Structures: Distribution of Intersegmental Resultants," Exercise Sport Sci. Rev., **9**(1), pp. 159–181.
[6] Herzog, W., 1996, "Force-Sharing Among Synergistic Muscles: Theoretical Considerations and Experimental Approaches," Exercise Sport Sci. Rev., **24**(1), pp. 173–202.
[7] Pandy, M. G., 2001, "Computer Modeling and Simulation of Human Movement," Annu. Rev. Biomed. Eng., **3**(1), pp. 245–273.
[8] Erdemir, A., McLean, S., Herzog, W., and van den Bogert, A. J., 2007, "Model-Based Estimation of Muscle Forces Exerted During Movements," Clin. Biomech., **22**(2), pp. 131–154.
[9] Pandy, M. G., and Andriacchi, T. P., 2010, "Muscle and Joint Function in Human Locomotion," Annu. Rev. Biomed. Eng., **12**(1), pp. 401–433.
[10] Martin, J. A., Brandon, S. C., Keuler, E. M., Hermus, J. R., Ehlers, A. C., Segalman, D. J., Allen, M. S., and Thelen, D. G., 2018, "Gauging Force by Tapping Tendons," Nat. Commun., **9**(1), pp. 1–9.
[11] Ates, F., Temelli, Y., and Yucesoy, C. A., 2014, "Intraoperative Experiments Show Relevance of Inter-Antagonistic Mechanical Interaction for Spastic Muscle's Contribution to Joint Movement Disorder," Clin. Biomech., **29**, pp. 943–949.
[12] Ates, F., Temelli, Y., and Yucesoy, C. A., 2016, "The Mechanics of Activated Semitendinosus Are Not Representative of the Pathological Knee Joint Condition of Children With Cerebral Palsy," J. Electromyography Kinesiology, **28**, pp. 130–136.
[13] Komi, P. V., Salonen, M., Järvinen, M., and Kokko, O., 1987, "In Vivo Registration of Achilles Tendon Forces in Man—I: Methodological Development," Int. J. Sports Med., **8**, pp. 3–8.
[14] Fukashiro, S., Komi, P. V., Järvinen, M., and Miyashita, M., 1993, "Comparison Between the Directly Measured Achilles Tendon Force and the Tendon Force Calculated From the Ankle Joint Moment During Vertical Jumps," Clin. Biomech., **8**(1), pp. 25–30.
[15] Sartori, M., Reggiani, M., Farina, D., and Lloyd, D. G., 2012, "EMG-Driven Forward-Dynamic Estimation of Muscle Force and Joint Moment About Multiple Degrees of Freedom in the Human Lower Extremity," PLoS One, **7**(12), p. e52618.
[16] Chao, E. Y. S., 2003, "Graphic-Based Musculoskeletal Model for Biomechanical Analyses and Animation," Med. Eng. Phys., **25**(3), pp. 201–212.
[17] Fisk, J. P., and Wayne, J. S., 2009, "Development and Validation of a Computational Musculoskeletal Model of the Elbow and Forearm," Ann. Biomed. Eng., **37**(4), pp. 803–812.
[18] Shelburne, K. B., Torry, M., and Pandy, M. G., 2005, "Muscle, Ligament, and Joint-Contact Forces at the Knee During Walking," Med. Sci. Sports Exercise, **37**(11), pp. 1948–1956.
[19] Schache, A. G., Dorn, T. W., Blanch, P. D., Brown, N. A., and Pandy, M. G., 2012, "Mechanics of the Human Hamstring Muscles During Sprinting," Med. Sci. Sports Exercise, **44**(4), pp. 647–658.
[20] Jastifer, J., Gustafson, P., Patel, B., and Uggen, C., 2012, "Pectoralis Major Transfer for Subscapularis Deficiency: A Computational Study," Shoulder Elbow, **4**(1), pp. 25–29.
[21] Homayouni, T., Underwood, K. N., Beyer, K. C., Martin, E. R., Allan, C. H., and Balasubramanian, R., 2015, "Modeling Implantable Passive Mechanisms for Modifying the Transmission of Forces and Movements Between Muscle and Tendons," IEEE Trans. Biomed. Eng., **62**(9), pp. 2208–2214.
[22] Correa, T. A., Schache, A. G., Graham, H. K., Baker, R., Thomason, P., and Pandy, M. G., 2012, "Potential of Lower-Limb Muscles to Accelerate the Body During Cerebral Palsy Gait," Gait Posture, **36**(2), pp. 194–200.
[23] Steele, K. M., DeMers, M. S., Schwartz, M. H., and Delp, S. L., 2012, "Compressive Tibiofemoral Force During Crouch Gait," Gait Posture, **35**(4), pp. 556–560.
[24] Rankin, J. W., Rubenson, J., and Hutchinson, J. R., 2016, "Inferring Muscle Functional Roles of the Ostrich Pelvic Limb During Walking and Running Using Computer Optimization," J. R. Soc. Interface, **13**(118), p. 20160035.
[25] Anderson, F. C., and Pandy, M. G., 2003, "Individual Muscle Contributions to Support in Normal Walking," Gait Posture, **17**(2), pp. 159–169.
[26] Liu, M., Anderson, F. C., Pandy, M. G., and Delp, S. L., 2006, "Muscles That Support the Body Also Modulate Forward Progression During Walking," J. Biomech., **39**(14), pp. 2623–2630.
[27] Pandy, M. G., Lin, Y. C., and Kim, H. J., 2010, "Muscle Coordination of Mediolateral Balance in Normal Walking," J. Biomech., **43**(11), pp. 2055–2064.
[28] Harrison, S. M., Whitton, R. C., King, M., Haussler, K. K., Kawcak, C. E., Stover, S. M., and Pandy, M. G., 2012, "Forelimb Muscle Activity During Equine Locomotion," J. Exp. Biol., **215**(17), pp. 2980–2991.
[29] McConnell, J., Donnelly, C., Hamner, S., Dunne, J., and Besier, T., 2012, "Passive and Dynamic Shoulder Rotation Range in Uninjured and Previously Injured Overhead Throwing Athletes and the Effect of Shoulder Taping," Am. J. Phys. Med. Rehabil., **4**, pp. 111–116.
[30] Gerus, P., Sartori, M., Besier, T. F., Fregly, B. J., Delp, S. L., Banks, S. A., Pandy, M. G., D'Lima, D. D., and Lloyd, D. G., 2013, "Subject-Specific Knee Joint Geometry Improves Predictions of Medial Tibiofemoral Contact Forces," J. Biomech., **46**(16), pp. 2778–2786.
[31] Lin, Y. C., Dorn, T. W., Schache, A. G., and Pandy, M. G., 2012, "Comparison of Different Methods for Estimating Muscle Forces in Human Movement," Proc. Inst. Mech. Eng., Part H., **226**(2), pp. 103–112.
[32] Bruno, A. G., Bouxsein, M. L., and Anderson, D. E., 2015, "Development and Validation of a Musculoskeletal Model of the Fully Articulated Thoracolumbar Spine and Rib Cage," ASME J. Biomech. Eng., **137**(8), p. 081003.

[33] Simonsen, E. B., and Komi, P. V., 2003, "Biomechanics of Locomotion," *Textbook of Sports Medicine Basic Science and Clinical Aspects of Sports Injury and Physical Activity*, M. Kjær, M. Krogsgaard, P. Magnusson, L. Engebretsen, H. Ross, T. Takala, and S. L. Y. Woo, eds., Blackwell Science, Hong Kong, China, pp. 107–133.
[34] Delp, S. L., Anderson, F. C., Arnold, A. S., Loan, P., Habib, A., John, C. T., Guendelman, E., and Thelen, D. G., 2007, "OpenSim: Open-Source Software to Create and Analyze Dynamic Simulations of Movement," IEEE Trans. Biomed. Eng., **54**(11), pp. 1940–1950.
[35] Schappacher-Tilp, G., Binding, P., Braverman, E., and Herzog, W., 2009, "Velocity-Dependent Cost Function for the Prediction of Force Sharing Among Synergistic Muscles in a One Degree of Freedom Model," J. Biomech., **42**(5), pp. 657–660.
[36] Herzog, W., and Leonard, T. R., 1991, "Validation of Optimization Models That Estimate the Forces Exerted by Synergistic Muscles," J. Biomech., **24**(Suppl. 1), pp. 31–39.
[37] Koppes, R. A., Herzog, W., and Corr, D. T., 2013, "Force Enhancement in Lengthening Contractions of Cat Soleus Muscle In Situ: Transient and Steady-State Aspects," Physiol. Rep., **1**(2), pp. 1–10.
[38] Thelen, D. G., and Anderson, F. C., 2006, "Using Computed Muscle Control to Generate Forward Dynamic Simulations of Human Walking From Experimental Data," J. Biomech., **39**(6), pp. 1107–1115.
[39] Kaya, M., Leonard, T., and Herzog, W., 2003, "Coordination of Medial Gastrocnemius and Soleus Forces During Cat Locomotion," J. Exp. Biol., **206**(20), pp. 3645–3655.
[40] Herzog, W., Leonard, T. R., and Guimaraes, A. C. S., 1993, "Forces in Gastrocnemius, Soleus, and Plantaris Tendons of the Freely Moving Cat," J. Biomech., **26**(8), pp. 945–953.
[41] Kaya, M., 2003, "Coordination of Cat Hindlimb Muscles During Voluntary Movements," Ph.D. thesis, University of Calgary, Calgary, AB, Canada.
[42] Kaya, M., Jinha, A., Leonard, T. R., and Herzog, W., 2005, "Multi-Functionality of the Cat Medial Gastrocnemius During Locomotion," J. Biomech., **38**(6), pp. 1291–1301.
[43] Walmsley, B., Hodgson, J. A., and Burke, R. E., 1978, "Forces Produced by Medial Gastrocnemius and Soleus Muscles During Locomotion in Freely Moving Cats," J. Neurophysiol., **41**(5), pp. 1203–1216.
[44] Merletti, R., 1999, "Standards for Reporting EMG Data," J. Electromyography Kinesiology, **9**, pp. 3–4.
[45] An, K. N., Takahashi, K., Harrigan, T. P., and Chao, E. Y., 1984, "Determination of Muscle Orientations and Moment Arms," ASME J. Biomech. Eng., **106**(3), pp. 280–282.
[46] Boyd, S. K., Muller, R., Leonard, T., and Herzog, W., 2005, "Long-Term Periarticular Bone Adaptation in a Feline Knee Injury Model for Post-Traumatic Experimental Osteoarthritis," Osteoarthritis Cartilage, **13**(3), pp. 235–242.
[47] Burkholder, T. J., and Nichols, T. R., 2004, "Three-Dimensional Model of the Feline Hindlimb," J. Morphol., **261**(1), pp. 118–129.
[48] O'Neill, M. C., Lee, L. F., Larson, S. G., Demes, B., Stern, J. T., Jr., and Umberger, B. R., 2013, "A Three-Dimensional Musculoskeletal Model of the Chimpanzee (Pan Troglodytes) Pelvis and Hind Limb," J. Exp. Biol., **216**, pp. 3709–3723.
[49] Thelen, D. G., 2003, "Adjustment of Muscle Mechanics Model Parameters to Simulate Dynamic Contractions in Older Adults," ASME J. Biomech. Eng., **125**(1), pp. 70–77.
[50] Young, R. P., Scott, S. H., and Loeb, G. E., 1993, "The Distal Hindlimb Musculature of the Cat: Multiaxis Moment Arms at the Ankle Joint," Exp. Brain Res., **96**(1), pp. 141–151.
[51] MacFadden, L. N., and Brown, N. A. T., 2007, "Biarticular Hip Extensor and Knee Flexor Muscle Moment Arms of the Feline Hindlimb," J. Biomech., **40**(15), pp. 3448–3457.
[52] MacFadden, L. N., and Brown, N. A. T., 2010, "The Influence of Modeling Separate Neuromuscular Compartments on the Force and Moment Generating Capacities of Muscles of the Feline Hindlimb," ASME J. Biomech. Eng., **132**(8), p. 081003.
[53] Sacks, R. D., and Roy, R. R., 1982, "Architecture of the Hind Limb Muscles of Cats: Functional Significance," J. Morphol., **173**(2), pp. 185–195.
[54] Zajac, F. E., 1989, "Muscle and Tendon: Properties, Models, Scaling, and Application to Biomechanics and Motor Control," Crit. Rev. Biomed. Eng., **17**(4), pp. 359–411.
[55] Anderson, F. C., and Pandy, M. G., 2001, "Static and Dynamic Optimization Solutions for Gait Are Practically Equivalent," J. Biomech., **34**(2), pp. 153–161.
[56] Luh, J. J., Chang, G. C., Cheng, C. K., Lai, J. S., and Kuo, T. S., 1999, "Isokinetic Elbow Joint Torques Estimation From Surface EMG and Joint Kinematic Data: Using an Artificial Neural Network Model," J. Electromyography Kinesiology, **9**(3), pp. 173–183.
[57] Ackland, D. C., Lin, Y. C., and Pandy, M. G., 2012, "Sensitivity of Model Predictions of Muscle Function to Changes in Moment Arms and Muscle-Tendon Parameters: A Monte Carlo Analysis," J. Biomech., **45**(8), pp. 1463–1471.
[58] Valero-Cuevas, F. J., Johanson, M. E., and Towles, J. D., 2003, "Towards a Realistic Biomechanical Model of the Thumb: The Choice of Kinematic Description Maybe More Critical Than the Solution Method or the Variability/Uncertainty of Musculoskeletal Parameters," J. Biomech., **36**(7), pp. 1019–1030.
[59] Hicks, J. L., Uchida, T. K., Seth, A., Rajagopal, A., and Delp, S. L., 2015, "Is My Model Good Enough? Best Practices for Verification and Validation of Musculoskeletal Models and Simulations of Movement," ASME J. Biomech. Eng., **137**(2), pp. 1–24.
[60] Bernstein, N. A., 1967, *The Co-Ordination and Regulation of Movements*, Pergamon Press, Oxford, New York.
[61] Crowninshield, R. D., and Brand, R. A., 1981, "A Physiologically Based Criterion of Muscle Force Prediction in Locomotion," J. Biomech., **14**(11), pp. 793–801.
[62] Wesseling, M., Derikx, L. C., de Groote, F., Bartels, W., Meyer, C., Verdonschot, N., and Jonkers, I., 2015, "Muscle Optimization Techniques Impact the Magnitude of Calculated Hip Joint Contact Forces," J. Orthop. Res., **33**(3), pp. 430–438.
[63] Lai, A. K., Arnold, A. S., and Wakeling, J. M., 2017, "Why Are Antagonist Muscles Co-Activated in My Simulation? A Musculoskeletal Model for Analysing Human Locomotor Tasks," Ann. Biomed. Eng., **45**(12), pp. 2762–2774.
[64] Redl, C., Gfoehler, M., and Pandy, M. G., 2007, "Sensitivity of Muscle Force Estimates to Variations in Muscle-Tendon Properties," Hum. Mov. Sci., **26**(2), pp. 306–319.